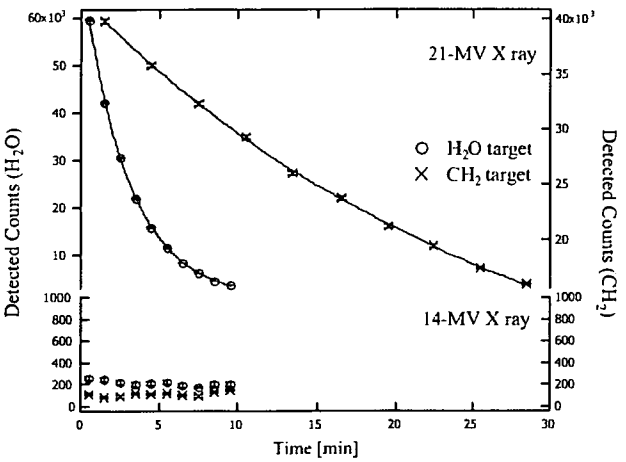

Fig. 6. Total annihilation gamma counts detected by PET-CT as a function of time for H_2O and CH_2 targets at two X-ray energies (21 MV and 14 MV). By way of curve fitting, the half-life for the H_2O target was found to be 122.5 s, which is in good agreement with the known half-life of ^{15}O. Similarly, the half-life for the CH_2 target was 18.8 min, which is also in good agreement with the known half-life of ^{11}C. No positron activity was detected at 14 MV

$$DC(T_m) \propto \begin{cases} 0.5^{T_m[\text{sec}]/122.5(\pm 1.4)} : \mathbf{H_2O} \\ 0.5^{T_m[\text{min}]/18.8(\pm 0.7)} : \mathbf{CH_2} \end{cases} \quad (5)$$

where DC stands for detection counts of annihilation gamma rays, and T_m is the time at measurement. The half-life for the H_2O target was 122.5 s, which is in good agreement with the known half-life of ^{15}O. The half-life for the CH_2 target was 18.8 min, which is also in good agreement with the known half-life of ^{11}C. At 14 MV, it was confirmed that no activity was detected.

In the present experiment, a dose of 17 Gy was required for PET image reconstruction. It is noted that 5 min were needed to move the phantom from the treatment room to the PET-CT room. During this period, the activity of ^{15}O reduces to 18% of the original activity owing to its short lifetime. If an on-line PET-CT was mounted to X-ray treatment equipment, a similar quality PET image along with a patient anatomy image could be obtained with a dose level of 3 Gy. It was estimated that on-beam line or in-irradiation room PET-CT imaging of ^{15}O positron emitter nuclei might provide the area of X-ray beam irradiation in a patient at a dose level of 3 Gy with X-ray beam energy of 21 MV.

Conclusions

The activity images of ^{15}O and ^{11}C positron emitter nuclei generated by 21-MV X-ray beam irradiation were able to provide the beam monitoring in a phantom and in a patient's body in this study.

Currently, the photon energies used for radiotherapy are mostly 6 MV and 10 MV. However, it is suggested that radiotherapy with a higher energy X-ray beam is suitable for tumors in areas such as the prostate, pelvis, and large liver. Also, when a high dose per fraction is irradiated in hypofractionated radiotherapy, the treatment period can be reduced.[26] Beam monitoring systems are important for high accuracy in radiotherapy, and confirmation of the irradiation area in a patient becomes possible using a high-energy X-ray beam beyond the threshold energy for the photonuclear reaction. Highly accurate in-vivo dose control in patients is currently difficult, but further development of photonuclear reaction-based dosimetry may help achieve this goal.

Acknowledgments. We thank the staff members of the Radiology Department of National Cancer Center, Kashiwa, for their assistance.

References

1. Takahashi S. Conformation radiotherapy: rotation techniques as applied to radiography and radiotherapy of cancer Acta Radiol Suppl 1965;242:1.
2. Brahme A. Optimization of stationary and moving beam radiation therapy techniques. Radiother Oncol 1988;12:129–40.
3. Yu C. Intensity-modulated arc therapy with dynamic multileaf collimation: an alternative to tomotherapy. Phys Med Biol 1995;40:1435–49.
4. Simpson RG, Chen CT, Grubbs EA, Swindell W. A 4-MV CT scanner for radiation therapy: the prototype system. Med Phys 1982;9:574–9.
5. Aoki Y, Akanuma A, Karasawa K, Sakata K, Nakagawa K, Muta N, et al. An integrated radiotherapy treatment system and its clinical application Radiat Med 1987;5:131-41.
6. Jaffray DA, Siewerdsen JH, Wong JW, Martinez AA. Flat-panel cone-beam computed tomography for image-guided radiation therapy. Int J Radiat Oncol Biol Phys 2002;53: 1337–49.
7. Ohara K, Okumura T, Akisada M, Inada T, Mori T, Yokota H, et al. Irradiation synchronized with respiration gate. Int J Radiat Oncol Biol Phys 1989;17:853–7.
8. Moore CH, Lilley F, Sauret V, Lalor M, Burton D. Optoelectronic sensing of body surface topology changes during radiotherapy for rectal cancer. Int J Radiat Oncol Biol Phys 2003; 56:248–58.
9. Tsunashima Y, Sakae T, Shioyama Y, Kagei K, Terunuma T, Nohtomi A, et al. Correlation between the respiratory waveform measured using a respiratory sensor and 3D tumor motion in gated radiotherapy. Int J Radiat Oncol Biol Phys 2004;60:951–8.
10. Shirato H, Shimizu S, Shimizu T, Nishioka T, Miyasaka K. Real-time tumor-tracking radiotherapy. Lancet 1999;353: 1331–2.
11. Sawada A, Yoda K, Kokubo M, Kunieda T, Nagata Y, Hiraoka M. A technique for noninvasive respiratory gated

radiation treatment system based on a real time 3D ultrasound image correlation: a phantom study. Med Phys 2004;31: 245–50.
12. Enghardt W, Fromm WD, Manfrass P, Schardt D. Limited angle 3D reconstruction of PET images for dose localization in light ion tumor therapy. Phys Med Biol 1992;37:791–8.
13. Litzenberg DW, Bajema JF, Becchetti FD, Brown JA, Raymond RS, Roberts DA, et al. On-line monitoring and PET imaging of proton radiotherapy beams. In: IEEE Medical Imaging Conference, Orlando, FL, 1992, pp 954–6.
14. Paans AMJ, Schippers JM. Proton therapy in combination with PET as monitor: a feasibility study. IEEE Trans Nucl Sci 1993;40:1041–4.
15. Litzenberg DW, Roberts DA, Lee MY, Pham K, Vander Molen AM, Ronningen R, et al. On-line monitoring of radiotherapy beams: experimental results with proton beams. Med Phys 1999;26:992–1006.
16. Nishio T, Ogino T, Nomura K, Uchida H. Dose-volume delivery guided proton therapy using beam on-line PET system. Med Phys 2006;33:4190–7.
17. Janek S. 3-Dimensional patient dose delivery verification based on PET-CT imaging of photonuclear reactions in 50 MV scanned photon beams. MSc thesis, Department of Medical Radiation Physics, Karolinska Institute and Royal Institute of Technology, 2002.
18. Brahme A. Biologically optimized 3-dimensional in vivo predictive assay-based radiation therapy using positron emission tomography-computerized tomography imaging. Acta Oncol 2003;42:123–36.
19. Uhrdin J, Janek S, Svensson R, Brahme A. 3D dose distribution in tissue calculated based on PET-CT imaging for high energy scanned photon therapy. Poster presentation, ESTRO, 2004.
20. Janek S. 3-Dimensional in vivo dose delivery verification by PET-CT imaging of photonuclear reactions in 50MV scanned photon beams. Series Internal Report. Department of Medical Radiation Physics, Karolinska Institute and Stockholm University, 2005, ISSN 1401-7466.
21. Muller H, Enghardt W. In-beam PET at high-energy photon beams. Phys Med Biol 2006;51:1779–89.
22. Photon, electron, proton and neutron interaction data for body tissues. ICRU Rep 1992;46:11–3.
23. National Nuclear Data Center, Brookhaven National Laboratory. Available at http://www.nndc.bnl.gov/.
24. Wu CS. The continuous X-rays excited by the beta-particles of ^{32}P. Phys Rev 1941;59:481–8.
25. Nishio T, Sato T, Kitamura H, Murakami K, Ogino T. Distributions of b^+ decayed nuclei generated in the CH_2 and H_2O targets by the target nuclear fragment reaction using therapeutic MONO and SOBP proton beam. Med Phys 2005;32: 1070–82.
26. Abratt RP, Bogart JA, Hunter A. Hypofractionated irradiation for non-small cell lung cancer. Lung Cancer 2002;36: 225–33.

Radiol Phys Technol (2008) 1:44–54
DOI 10.1007/s12194-007-0008-8

Experimental verification of proton beam monitoring in a human body by use of activity image of positron-emitting nuclei generated by nuclear fragmentation reaction

Teiji Nishio · Aya Miyatake · Kazumasa Inoue · Tomoko Gomi-Miyagishi · Ryosuke Kohno · Satoru Kameoka · Keiichi Nakagawa · Takashi Ogino

Received: 2 July 2007 / Revised: 22 October 2007 / Accepted: 23 October 2007 / Published online: 27 November 2007

Abstract Proton therapy is a form of radiotherapy that enables concentration of dose on a tumor by use of a scanned or modulated Bragg peak. Therefore, it is very important to evaluate the proton-irradiated volume accurately. The proton-irradiated volume can be confirmed by detection of pair-annihilation gamma rays from positron-emitting nuclei generated by the nuclear fragmentation reaction of the incident protons on target nuclei using a PET apparatus. The activity of the positron-emitting nuclei generated in a patient was measured with a PET-CT apparatus after proton beam irradiation of the patient. Activity measurement was performed in patients with tumors of the brain, head and neck, liver, lungs, and sacrum. The 3-D PET image obtained on the CT image showed the visual correspondence with the irradiation area of the proton beam. Moreover, it was confirmed that there were differences in the strength of activity from the PET-CT images obtained at each irradiation site. The values of activity obtained from both measurement and calculation based on the reaction cross section were compared, and it was confirmed that the intensity and the distribution of the activity changed with the start time of the PET imaging after proton beam irradiation. The clinical use of this information about the positron-emitting nuclei will be important for promoting proton treatment with higher accuracy in the future.

Keywords Proton therapy · Proton beam monitoring · Beam OFF-LINE PET system · PET-CT imaging

T. Nishio (✉) · T. Gomi-Miyagishi · R. Kohno · S. Kameoka · T. Ogino
Particle Therapy Division, Research Center for Innovative Oncology, National Cancer Center, Kashiwa, 6-5-1 Kashiwano-ha, Kashiwa-shi, Chiba 277-8577, Japan
e-mail: tnishio@east.ncc.go.jp

T. Nishio · A. Miyatake
Department of Nuclear Engineering and Management, Graduate School of Engineering, University of Tokyo, 2-11-16 Yayoi, Bunkyo-ku, Tokyo 113-0032, Japan

T. Nishio · K. Nakagawa
Department of Radiology, Graduate School of Medicine, University of Tokyo, 7-3-1 Hongo, Bunkyo-ku, Tokyo 113-8655, Japan

K. Inoue
Department of Radiology, National Cancer Center, Kashiwa, 6-5-1 Kashiwano-ha, Kashiwa-shi, Chiba 277-8577, Japan

Present Address:
K. Inoue
Functional Imaging Division, Research Center for Innovative Oncology, National Cancer Center, Kashiwa, 6-5-1 Kashiwano-ha, Kashiwa-shi, Chiba 277-8577, Japan

K. Inoue
Graduate School of Health Science, Tokyo Metropolitan University, 7-2-10 Higashiogu, Arakawa-ku, Tokyo 116-8551, Japan

1 Introduction

Proton therapy has allowed the dose to be concentrated only on a tumor. The use of proton therapy is spreading throughout the world as a highly accurate method of radiation therapy [1]. In the future, proton therapy will be expected to become one of the main forms of radiation therapy because of its high utility. On the other hand, the diagnosis of an initial or small tumor has become

possible with developments in imaging methods that provide high resolution and contrast. In particular, positron emission tomography (PET) has advanced rapidly, and its use has become widespread. PET-computed tomography (CT) combines PET and CT and is now readily available. The fusion of PET and CT images can be achieved with high precision by use of a PET-CT apparatus. As a result, the location of activity can be determined with high accuracy.

In this study, the activity of positron-emitting nuclei generated by the nuclear fragmentation reaction of incident protons and nuclei constituting of a patient body was measured with a PET-CT apparatus (beam OFF-LINE PET system), and the proton-irradiated volume was confirmed. So far most researches were limited to phantom studies using a PET apparatus (no combined with CT apparatus) [2–13]. Verification of activity measurement was performed in patients with tumors of the brain, head and neck, liver, lungs, and sacrum. By use of a fusion imaging obtained with a combined PET-CT apparatus, the irradiated volume was confirmed immediately after proton therapy with higher accuracy than that the use of fusion of images obtained from the separate PET apparatus and CT apparatus.

We are researching dose-volume delivery-guided proton therapy (DGPT) for confirmation of the proton-irradiated volume and dose distribution by using a beam ON-LINE PET system (BOLPs) in the proton treatment room [13]. The activity image of each treatment site obtained with the PET-CT apparatus will be used for the simulation and estimation of the activity image acquired from the BOLPs immediately after proton irradiation to a patient.

This paper is organized as follows. Experimental procedures are described in Sect. 2. Measurement and analysis results and discussion are presented in Sect. 3. Section 4 discusses the conclusions of this study regarding proton therapy.

2 Materials and methods

2.1 Nuclear fragmentation reaction of incident protons and target nuclei

The nuclear fragmentation reaction occurs in the human body by high-energy proton beam irradiation during proton therapy. Many kinds of nuclei, including positron-emitting nuclei, are generated by the reaction.

The activity $N_{\beta+}$ of the positron-emitting nuclei Y generated from each type of tissue composition by the nuclear fragmentation reaction is expressed as the following equation [11]:

$$N_{\beta+}(tissue;E_p)\,[\mathrm{kBq/cc/GyE}] = \Phi_p(tissue;E_p) \cdot \sum_X \sum_Y \left| \begin{array}{l} \frac{1}{T_m} \cdot \left\{1-\exp\left(-\sigma_{X\to Y}(E_p)\cdot n_{tissue}(X)\cdot \Delta_{tissue}\right)\right\} \\ \times \left\{\frac{T_{1/2}(Y)}{T_i\cdot \ln 2}\cdot\left(1-2^{-T_i/T_{1/2}}(Y)\right)\right\} \\ \times 2^{-T_0/T_{1/2}}(Y)\times\left(1-2^{-T_m/T_{1/2}}(Y)\right) \end{array} \right| . \quad (1)$$

Here, X denotes the target nuclei in the tissue, z the depth, T_m the time of the activity measurement, T_i the time of the proton irradiation, T_0 the interval between the start of the activity measurement and the discontinuation of proton irradiation, and $T_{1/2}$ the half life of the generated positron-emitting nuclei. The reaction cross section of $\sigma_{X\to Y}$, which determines the rate of generation in the nuclear fragmentation reaction $X(p,x)Y$, depends on the kind of target nucleus (mass number A_t, atomic number Z_t) and the relative kinetic energy of E_p. n_{tissue} denotes the number per unit volume of the nucleus in the tissue, and Δ_{tissue} the target thickness. Data of human body composition are based on ICRU Report 46 [14]. The number of incident protons per the dose and the volume Φ_p, is expressed as follows:

$$\Phi_p(tissue;E_p)\,[\mathrm{protons/cc/GyE}] = 1\times 10^{-3} \Big/ \left\{\left(dE_p/dx[\mathrm{J/cm}]\right)\cdot RBE\right\} = \left[1.671\times 10^{-11}\cdot\left\{\frac{\ln\left(1.363\times 10^4\cdot\left(\gamma(E_p)^2-1\right)\right)}{\beta(E_p)^2}-1\right\}\right]^{-1} . \quad (2)$$

Here, RBE is the relative biological effectiveness. β and γ are expressed by use of the kinetic energy of the proton, in the following equation:

$$\beta(E_p) = \sqrt{1-\frac{1}{\left(1+1.066\times 10^{-3}\cdot E_p\right)^2}},$$
$$\gamma(E_p) = 1+1.066\times 10^{-3}\cdot E_p. \quad (3)$$

The ^{12}C, ^{14}N, ^{16}O, and ^{40}Ca nuclei are main chemical elements of the human body [14]. For proton therapy, the number of each positron-emitting nuclei, generated in the human body depends on the target nuclei and on the incident proton beam energy.

Some the experimental data of the reaction for $^{12}C(p,x)Y$, $^{14}N(p,x)Y$, $^{16}O(p,x)Y$ have been reported [15]. The mean values of the reaction cross sections of the ^{11}C, ^{13}N, and ^{15}O nuclei generated from the ^{12}C and ^{16}O nuclei are especially expressed as follows [11]:

$$\sigma_{X\to Y}(E_p) = \frac{a}{1+\exp\left(\frac{b-E_p}{c}\right)} \cdot \left\{1 - d\cdot\left(1 - e\cdot\exp\left(-\frac{E_p - f}{g}\right)\right)^h\right\},$$

X	Y	a	b	c	d	e	f	g	h
^{12}C	^{11}C	96.0	21.4	0.9	0.5	1.2	39.0	34.5	2.0
^{16}O	^{15}O	71.0	26.0	2.8	0.6	1.1	41.0	36.0	6.0
^{16}O	^{13}N	66.0	10.4	0.4	0.9	0.8	11.6	6.8	1.0
^{16}O	^{11}C	18.8	43.6	3.6	0.5	1.0	49.0	35.0	4.0

(4)

Here, the reaction cross section of $\sigma_{X\to Y}$ and the relative kinetic energy E_p have units of mb and MeV, respectively. The letters a, ..., h are constant parameters for the calculation of the reaction cross section in each reaction channel. The data of the reaction for ^{40}Ca(p,x)Y is mainly calculated with the INTENSITY code [16, 17] because there is no experiment value.

2.2 Proton therapy at each treatment site

The proton radiotherapy facility of the National Cancer Center, Kashiwa has a small normal-conducting AVF cyclotron (C235) for medical purposes, two rotating gantry ports, and one horizontal fixed port [18, 19]. For obtaining laterally uniform irradiation fields, the dual-ring double scattering method is used in one rotating gantry port and the horizontal fixed port; the wobbler method is used with the other rotating port. The uniform proton dose distribution during proton treatment is controlled by a simple feed back control system equipped with an automatic fine adjustment of the beam axis and a mechanism for moving the second dual-ring scatter of the double scatters to the optimal position [20]. Using this system, we achieved uniform dose distribution in the irradiation field during proton radiotherapy, with symmetry within ±1% and flatness within 2%. The accuracy of the calculated dose is similarly proportional to the accuracy of the measured and calculated activities.

Verification of the activity measurement was performed in about 20 cases with tumors of the brain, head and neck, liver, lungs, and sacrum. Proton beam irradiation to the liver and lung was performed with synchronization to the respiratory motion of the target organ. The position uncertainty of the target organ is within 5 mm. The proton treatment planning system, PTPLAN/ndose, developed in our facility [21] was used for planning of the proton treatment. The accuracy of the proton range is estimated within 3 mm in conversion of Hounsfield units (HU) of the planning CT image to water equivalent length. The accuracy of the dose calculation will be within 5% for the homogeneous or simply inhomogeneous body (e.g., prostate, liver, lung), and be greater than 10% at the boundary of the inhomogeneous tissue (e.g., head and neck). The dose calculation was performed with the margin of the 3 mm for the brain and the head and neck, and 5 mm for the liver, the lung, and the prostate.

2.3 Measurement of activity with PET-CT apparatus

The activity of the positron-emitting nuclei generated in the patients by proton beam irradiation was measured with the PET-CT apparatus (Discovery ST (GE Medical Systems, Milwaukee, Wisconsin, U.S.A.)) at our institution. The PET-CT apparatus was a detection system with 10,080 BGO (Bismuth-Germanium-Oxide) with a crystal size of 6.2 × 6.2 × 30 mm^3 arranged on a circumference of a circle with a diameter of 88.6 cm. 3D reconstruction algorithm of OSEM (Ordered Subsets Expectation Maximization) was employed with a position resolution of 5.0–6.7 mm, which was position-dependent. The axial size of the field of view (FOV) was 15.7 cm. The accuracy of the absolute activity measured with the commercial PET-CT apparatus has been reported to be commonly about 10% [22].

The distance between the room for proton treatment and the room with the PET-CT apparatus was about 40 m. Therefore, PET scanning was started about 7 min after irradiation, and the image was acquired over 5 min. Therefore, the biological washout effect in the metabolism of a living tissue is important for the verification of the absolute activity and the activity distribution of the positron-emitting nuclei induced by the proton irradiation. In studies in which the radioactive ion beam (^{11}C,^{10}C) to a rabbit was irradiated, the decay curve has three components of a fast decay (decay constant ~2–10 s), medium decay (decay constant ~100–200 s), and slow decay (decay constant ~3,000–10,000 s) [23, 24]. The 50–65% of total activity is the fast and medium components.

The proton beam was irradiated to the tumor in the liver and lungs with the beam synchronized to respiratory motion. However, the activity of the positron-emitting nuclei generated in the patient was measured without synchronizing to respiratory motion of the target organ. The corresponding tumor movement will be a few cm.

3 Results and discussion

3.1 Visual verification of PET-CT image at each treatment site

The measured activity distribution and the calculated dose distribution on CT image for proton treatment of a tumor in the sacrum as one of the site studies are shown in Fig. 1. Proton beam irradiation was performed with a gantry angle of 180 degrees and a dose of 2.5 GyE [= [Gy] x *RBE* (= 1.1 = constant)]. Moreover, the width of the spread-out Bragg peak (SOBP) was 70 mm. The activity fitted on the area of proton irradiation was visually confirmed by comparison with the proton dose distribution. The activity observed in the proton irradiated area of subcutaneous adipose tissue and bone tissue was higher than that in the surrounding area.

Figure 2 shows the results for prostate tumor. Proton beam irradiation was performed with a gantry angle of 90°, a SOBP width of 60 mm, and a dose of 2.0 GyE. Similarly, high activity was observed in the subcutaneous adipose tissue and in the femur.

Figure 3 shows the results for a tumor of the head and neck. Proton beam irradiation was performed twice with each dose of 2.0-GyE, and a gantry angle of 230° for the initial exposure, followed by 330° for the second one. The respective widths of the SOBP were 80 and 70 mm. The interval between the two irradiation procedures was about 9 min. Therefore, the activity of the 330° proton beam was higher than that of the 230° beam. High activity was similarly observed in the areas of adipose tissue and maxilla irradiated by the proton beam.

Figure 4 shows the results for a liver tumor. Proton beam irradiation was performed with a 3.8-GyE dose and 80 mm SOBP from a gantry angle of 290°. During treatment, the proton beam irradiation was synchronized to the respiratory motion of the target organ. However, during the acquisition of PET-CT image data, there was no synchronization to the respiratory motion. Similarly, high activity was observed in the area of subcutaneous adipose tissue. The findings of activity during proton treatment after a transarterial chemoembolization therapy (TACE) procedure using lipiodol for a liver tumor are shown in Fig. 5. The CT value of 80–350 HU in area including the lipiodol is considerably higher than 70 HU in a normal liver. Proton beam irradiation was performed with a 3.8-GyE dose and 80 mm SOBP at a gantry angle of 180°. The activity in the liver tumor was high. We speculated that this was because many positron-emitting nuclei were generated from the iodine nuclei contained in the lipiodol.

3.2 Specificity of activity generated in each body tissue

The activity in each tissue and the interval between beam-stop time and start-time of activity measurement was calculated from Eq. 1. A beam irradiation time of 2 min and the beam energy in each tissue are used in the calculation. The reaction cross sections of $^{12}C(p,x)^{11}C$, $^{16}O(p,x)^{15}O$, $^{16}O(p,x)^{13}N$, and $^{16}O(p,x)^{11}C$ reactions were calculated from Eq. 4 at each proton energy. The reaction cross sections of $^{12}C(p,x)^{10}C$, $^{16}O(p,x)^{14}O$, $^{40}Ca(p,x)^{38}K$, $^{40}Ca(p,x)^{30}P$, $^{40}Ca(p,x)^{15}O$, $^{40}Ca(p,x)^{13}N$, and $^{40}Ca(p,x)^{11}C$ reactions were calculated with the INTENSITY code. For

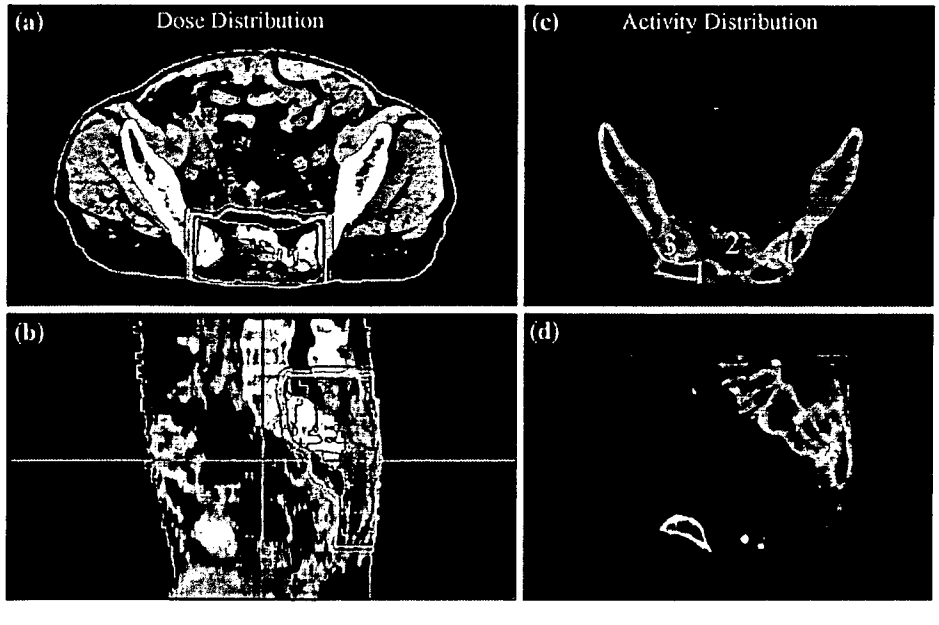

Fig. 1 Dose distribution calculated with the proton treatment planning system and activity measured with the PET-CT apparatus on CT image after proton treatment of tumor in the sacrum. The iso-dose line of 100% is red, 80% yellow green, 50% light blue, and 20% purple. The activity line of 5 kBq/cc is red, 3 kBq/cc green, and 1 kBq/cc bule. Proton beam irradiation was performed with an SOBP of 70 mm, gantry angle of 180°, and dose of 2.5 GyE. The dose distributions on each CT image in axial and coronal planes are shown in figures (a) and (b), and the activity are shown in figures (c) and (d)

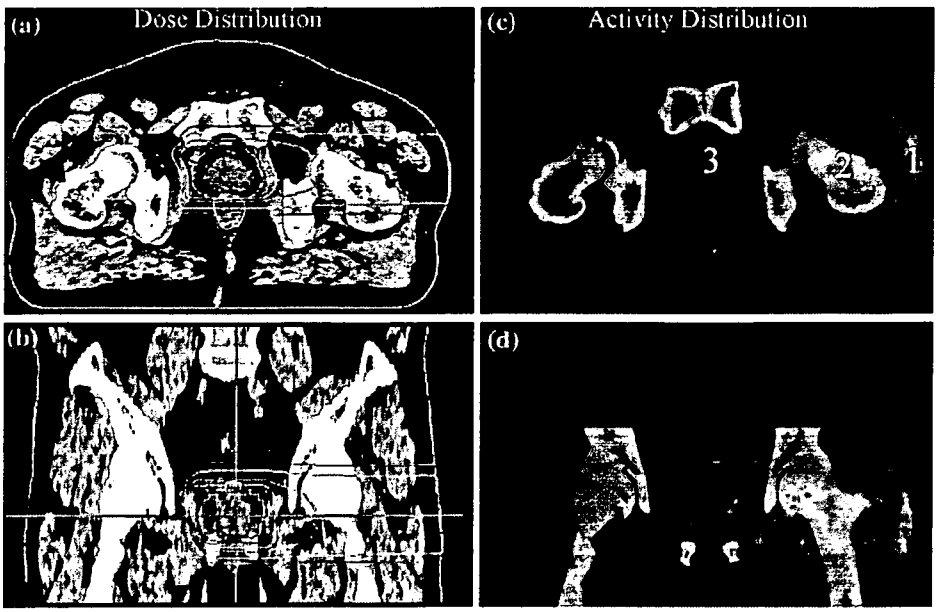

Fig. 2 Dose distribution calculated with the proton treatment planning system and activity measured with the PET-CT apparatus on CT image after proton treatment of tumor in the prostate. The iso-dose line of 100% is red, 80% yellow green, 50% light blue, and 20% purple. The activity line of 5 kBq/cc is red, 3 kBq/cc green, and 1 kBq/cc bule. Proton beam irradiation was performed with an SOBP of 60 mm, gantry angle of 90°, and dose of 2.0 GyE. The dose distributions on each CT image in axial and coronal planes are shown in figures (**a**) and (**b**), and the activity are shown in figures (**c**) and (**d**)

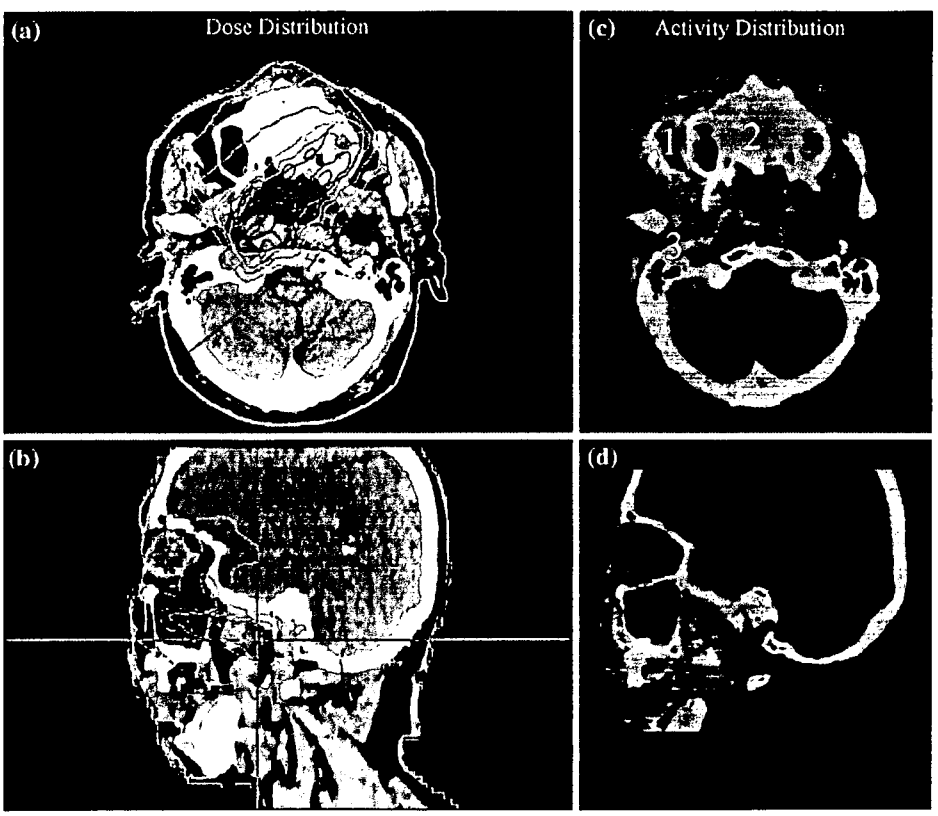

Fig. 3 Dose distribution calculated with the proton treatment planning system and activity measured with the PET-CT apparatus on CT image after proton treatment of tumor in the head and neck. The iso-dose line of 100% is red, 80% yellow green, 50% light blue, and 20% purple. The activity line of 5 kBq/cc is red, 3 kBq/cc green, and 1 kBq/cc bule. Proton beam irradiation was performed with an SOBP of 70 mm, gantry angle of 330°, and dose of 2.0 GyE after irradiation with an SOBP of 80 mm, gantry angle of 230°, and dose of 2.0 GyE. The dose distributions on each CT image in axial and coronal planes are shown in figures (**a**) and (**b**), and the activity are shown in figures (**c**) and (**d**)

$^{14}N(p,x)^{13}N$, $^{14}N(p,x)^{11}C$, and $^{14}N(p,x)^{10}C$ reactions, experimental data [15] were used. The results are shown in Fig. 6. Data of each human body composition and the proton energy used for the calculation of the time dependent activity in various tissues are shown in Table 1. The activity of adipose tissue was higher than that in the liver more than 6 min after proton beam irradiation. The same tendency was shown for activity measurements with use of the PET-CT apparatus after proton treatment for liver cancer.

The calculated decay curve is approximated with two components of short (^{15}O, ^{14}O, ...) and long (^{13}N, ^{11}C, ...) half life, and is expressed as the following equation:

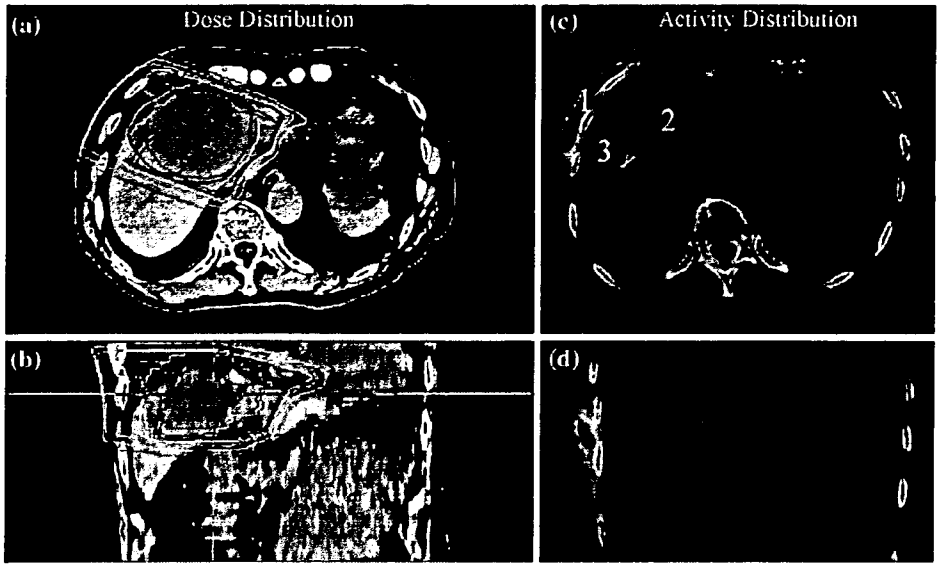

Fig. 4 Dose distribution calculated with the proton treatment planning system and activity measured with the PET-CT apparatus on CT image after proton treatment of tumor in the liver. The iso-dose line of 100% is red, 80% yellow green, 50% light blue, and 20% purple. The activity line of 7 kBq/cc is red, 5 kBq/cc green, and 3 kBq/cc bule. The proton beam irradiation was performed with an SOBP of 80 mm, gantry angle of 290°, and dose of 3.8 GyE. The dose distributions on each CT image in axial and coronal planes are shown in figures (**a**) and (**b**), and the activity are shown in figures (**c**) and (**d**)

$$N_{\beta+}(Tissue;T_0)[\mathrm{kBq/cc/GyE}] = \begin{cases} 2.2\times 2^{-T_0[\mathrm{min}]/1.9}+0.6\times 2^{-T_0[\mathrm{min}]/17.7} & (\mathrm{Tumor}) \\ 3.1\times 2^{-T_0[\mathrm{min}]/2.0}+0.5\times 2^{-T_0[\mathrm{min}]/16.8} & (\mathrm{Liver}) \\ 1.4\times 2^{-T_0[\mathrm{min}]/1.9}+0.8\times 2^{-T_0[\mathrm{min}]/18.6} & (\mathrm{Adipose\ Tissue}) \\ 5.9\times 2^{-T_0[\mathrm{min}]/2.0}+1.6\times 2^{-T_0[\mathrm{min}]/17.8} & (\mathrm{Skeleton\ Cranium}) \\ 3.0\times 2^{-T_0[\mathrm{min}]/1.9}+1.4\times 2^{-T_0[\mathrm{min}]/17.8} & (\mathrm{Skeleton\ Femur}) \\ 4.3\times 2^{-T_0[\mathrm{min}]/1.9}+1.3\times 2^{-T_0[\mathrm{min}]/17.4} & (\mathrm{Skeleton\ Ribs}) \end{cases} \quad (5)$$

The value of short or long half life in each tissues was consistent within 5% accuracy, and was equal to the our study using a dead rabbit [13]. This result showed that the activity at $T_0 = 0$ (condition of the measurement in the BOLPs) was higher five times than that at $T_0 = 7$ min (condition of this work in the commercial PET-CT apparatus).

Figure 7 shows the ratio R of the calculated activity normalized to one at $T_0 = 0$. It is expressed as the following equation:

$$R(tissue;T_0) = \frac{N_{\beta+}(Tumor;T_0=0)}{N_{\beta+}(Tissue;T_0=0)} \cdot \frac{N_{\beta+}(Tissue;T_0)}{N_{\beta+}(Tumor;T_0)}. \quad (6)$$

The results showed that the image of the activity changed during $T_0 = 0 \sim 10$ min. Therefore, the observed image of off-line PET (commercial PET-CT apparatus) will be different from that of the on-line PET (BOLPs).

The value of the activity at points 1, 2, and 3 on the axial activity images are shown in Figs. 1, 2, 3, 4 and 5. The points were selected on the soft tissue (tumor), the subcutaneous adipose tissue, and the bone tissue. The reaction cross sections, the kinetic energies of the proton beam at each point, and the half lives of the positron-emitting nuclei are shown in Table 2. The irradiation dose, irradiation time, interval between discontinuing the beam and acquiring the PET image, and the measured, the calculated value (Calculation: B) and the differences of activity at the point are summarized in Table 3.

It was estimated that the measured activity had a statistical accuracy of 9% (2 kBq/cc at 10 cm path length in the human body, 5 min measurement, each cubic voxel with a perimeter of 4 mm), and the image reconstruction accuracy was 10%. The accuracy of the measured activity in the biological washout effect is estimated to be very large, and is difficult to show the correspondence quantitatively. Moreover, the coefficient of the effect is always smaller than one. In the calculated activity, the accuracy of the reaction cross sections and the number of incident protons were estimated to be 20 and 5%, respectively. In the soft tissue and the liver, the measurement and the calculation activity were consistent within the error bar. On the other hand, the measured activity was about two to four times as large as the calculated activity in the adipose tissue, and about two times that in the femur. In the high activity of the adipose tissue, the accuracy of the attenuation correction factor of the 511-keV gamma ray based on the CT value of the subcutaneous adipose tissue under the adjacent body surface will partly influence the discrepancy in the activity measurement. The high activity of the femur was probably due to the accuracy of the calculation based on the fragmentation reaction cross section of ^{40}Ca. In the liver tumor after a TACE procedure with lipiodol, the measured activity was about four times as large as the calculated activity in the case without the lipiodol. It is noted that the nuclear fragmentation reaction of the iodine contained in the lipiodol is unknown well.

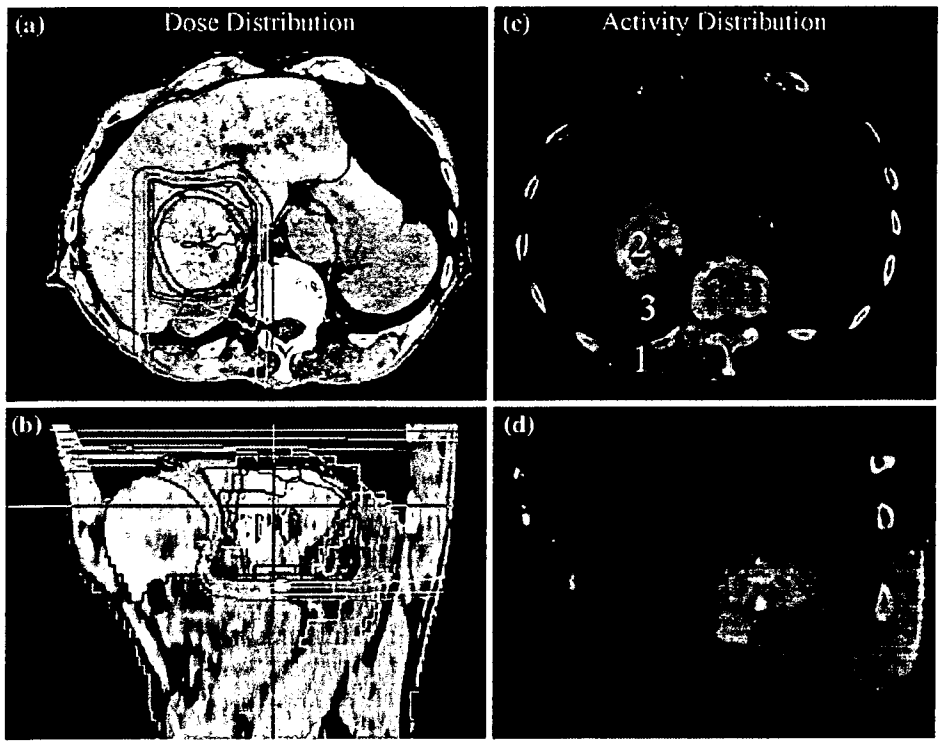

Fig. 5 Dose distribution calculated with the proton treatment planning system and activity measured with the PET-CT apparatus on CT image after proton treatment of liver tumor following TACE. The iso-dose line of 100% is red, 80% yellow green, 50% light blue, and 20% purple. The activity line of 7 kBq/cc is red, 5 kBq/cc green, and 3 kBq/cc bule. Proton beam irradiation was performed with an SOBP of 80 mm, gantry angle of 180 degrees and dose of 3.8 GyE. The dose distributions on each CT image in axial and coronal planes are shown in figures (a) and (b), and the activity are shown in figures (c) and (d)

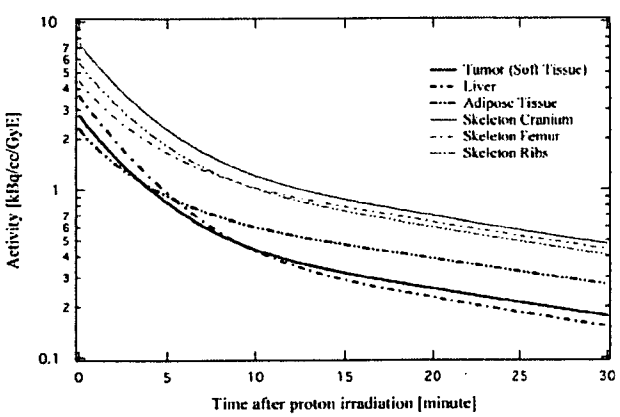

Fig. 6 Calculated activity $N_{\beta+}$ to the interval between the stopping beam and starting measurement of the activity in various tissues

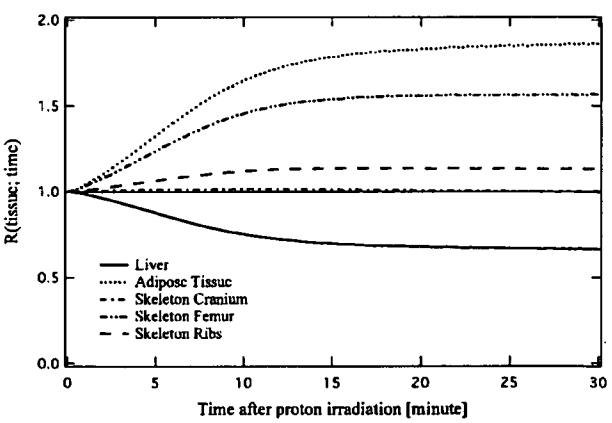

Fig. 7 Ratio R of the calculated activity normalized to one at $T_0 = 0$ in various tissues

Table 1 Data of human body composition and proton energy used for the calculation of the time dependent activity in various tissues

Body tissue	n_{tissue} (X)(10^{22}/cm^3)					Proton energy (MeV)
	H	C	N	O	Other (Ca)	
Tumor (soft tissue)	6.6	1.3	0.1	2.4	0.0	60.4
Liver	6.6	0.7	0.1	2.9	0.0	70.6
Adipose tissue	6.6	2.5	0.1	1.3	0.0	114.3
Skeleton cranium	5.9	2.1	0.3	3.2	0.3	89.1
Skeleton femur	6.4	2.6	0.2	2.1	0.1	141.6
Skeleton ribs	6.3	2.1	0.3	2.7	0.2	109.6

"Calculation: C" in Table 3 is the calculated activity in the simulation of the 5 min measurement with a PET apparatus immediately after the proton irradiation. As a result, it was estimated that the activity was about 10 kBq/cc per 2.5-GyE dose immediately after the proton irradiation.

The biological washout effect will greatly affect the accuracy of the measured activity. The coefficient of the effect has been estimated to be the 50–65% of total activity [23, 24]. However, the radioactive ion beam was irradiated to a living tissue in the study. A flow-out of the positron-emitting nuclei implanted by the radioactive ion

Table 2 Proton energy, reaction cross section, half life used for the calculation of the activity in human body

Treatment site	Interest point	Proton energy (MeV)	Irradiation dose (GyE)	Cross section (mb)														
				Target nuclei	^{12}C	^{12}C	^{14}N	^{14}N	^{14}N	^{16}O	^{16}O	^{16}O	^{16}O	^{16}O	^{40}Ca	^{40}Ca	^{40}Ca	^{40}Ca	^{40}Ca
				PositronEmitting nuclei	^{11}C	^{10}C	^{13}N	^{11}C	^{10}C	^{15}O	^{14}O	^{13}N	^{11}C	^{10}C	^{38}K	^{30}P	^{15}O	^{13}N	^{11}C
				Half life (min)	20.39	0.321	9.965	20.39	0.321	2.037	1.177	9.965	20.39	0.321	7. 636	2.498	2.037	9.965	20.39
Sacrum	1	73.1	2.5		81.3	4.4	16.1	52.4	6.5	69.8	1.7	6.6	18.2	1.8	14.1	9.2	2.2	2.2	2.2
	2	48.4	2.5		95.6	5.2	24.1	65.3	8.0	71.0	1.7	6.8	14.9	1.9	14.1	9.2	2.2	2.2	2.2
	3	62.1	2.5		88.9	4.8	6.6	18.6	1.9	70.9	1.7	6.6	18.6	1.9	14.1	9.2	2.2	2.2	2.2
Prostate	1	173.0	1.4		50.3	2.7	8.1	13.7	1.7	35.1	0.8	6.6	10.4	0.9	14.1	9.2	2.2	2.2	2.2
	2	137.7	1.4		54.4	2.9	14.9	11.6	1.4	44.3	1.1	6.6	12.1	1.2	14.1	9.2	2.2	2.2	2.2
	3	63.3	2.0		88.1	4.8	19.0	58.6	7.2	70.8	1.7	6.6	18.6	1.9	14.1	9.2	2.2	2.2	2.2
Head and neck	1	103.3	2.7		64.2	3.5	12.3	33.3	4.1	59.4	1.4	6.6	15.2	1.6	14.1	9.2	2.2	2.2	2.2
	2	70.4	3.7		83.2	4.5	16.9	54.1	6.7	70.2	1.7	6.6	18.4	1.9	14.1	9.2	2.2	2.2	2.2
	3	115.9	1.7		59.6	3.2	13.2	25.4	3.1	53.4	1.3	6.6	13.8	1.4	14.1	9.2	2.2	2.2	2.2
Liver	1	121.1	3.2		58.1	3.1	13.6	22.1	2.7	51.1	1.2	6.6	13.4	1.3	14.1	9.2	2.2	2.2	2.2
	2	75.9	3.8		79.4	4.3	15.2	50.6	6.2	69.3	1.6	6.6	18.0	1.8	14.1	9.2	2.2	2.2	2.2
	3	100.8	3.8		65.3	3.5	12.1	34.9	4.3	60.6	1.4	6.6	15.5	1.6	14.1	9.2	2.2	2.2	2.2
Liver	1	131.9	3.1		55.5	3.0	14.5	15.3	1.9	46.5	1.1	6.6	12.5	1.2	14.1	9.2	2.2	2.2	2.2
	2	71.8	3.8		82.2	4.4	16.5	53.2	6.6	70.0	1.7	6.6	18.3	1.8	14.1	9.2	2.2	2.2	2.2
	3	110.0	3.4		61.6	3.3	12.8	29.1	3.6	56.2	1.3	6.6	14.5	1.5	14.1	9.2	2.2	2.2	2.2

beam is the washout effect. On the other hand, in our study, the positron-emitting nuclei are generated from the nuclei in a tissue constituting a human body. Therefore, physiology, the effect has a different possibility. Perhaps, it is guessed that the effect may be not too large at our study.

The measured and calculated activities summarized in Table 3 will have the large error bar of a few 10%, and be scarcely correspondent within the large error bar in the soft tissue and the bone tissue except a skeleton femur. The measured activities in the subcutaneous adipose tissue, the skeleton femur, and the liver tumor after a TACE procedure are about two to three times higher than the calculated activities. Anyway the reason of large disagreement is not clear.

3.3 Comparison between proton dose distribution and activity distribution

The activity distribution visually corresponded to the proton dose distribution in Figs. 1, 2, 3, 4 and 5. Figure 8 shows the dose and activity distributions with a spike shape on the sagittal CT image in the head and neck. The position of the dose and activity distributions of the spike shape was consistent. However, it is difficult to show the correspondence quantitatively. We have executed the quantitative evaluation concerning the correspondence of the proton dose distribution and the activity distribution by our previous research [11, 13]. As the results, the activity range was about 7 mm shorter in a water equivalent length than the proton range expected from the energy threshold for the

Table 3 Proton irradiation dose, irradiation time, time of activity measurement, and level of activity measured and calculated

Treatment site	Irradiation dose (GyE/fx.)	Irradiation time (s)	Interval between stopping beam and starting measurment (s)	Point	Irradiation dose (GyE)	Activity (kBq/cc)		A/B	Activity (kBq/cc)
						Measurement:A	Calculation:B		Calculation:C
Sacrum	2.5	55	430	1	2.5	3.8(± 0.5)	1.7(± 0.4)	2.2(± 0.6)	5.5(± 1.2)
				2	2.5	1.8(± 0.2)	2.1(± 0.4)	0.9(± 0.5)	8.5(± 1.8)
				3	2.5	2.5(± 0.3)	2.5(± 0.5)	1.0(± 0.6)	10.2(± 2.1)
Prostate	2.0	41	450	1	1.4	4.6(± 0.6)	1.1(± 0.2)	4.2(± 0.7)	3.3(± 0.7)
				2	1.4	4.2(± 0.6)	1.8(± 0.4)	2.3(± 0.7)	6.7(± 1.4)
				3	2.0	1.2(± 0.2)	1.3(± 0.3)	0.9(± 0.3)	6.1(± 1.3)
Head and neck	4.0	45	436	1	2.7	4.4(± 0.6)	1.7(± 0.4)	2.6(± 0.7)	3.0(± 0.6)
				2	3.7	3.0(± 0.4)	4.1(± 0.9)	0.7(± 0.9)	25.1(± 5.2)
				3	1.7	1.1(± 0.1)	1.4(± 0.3)	0.8(± 0.3)	13.1(± 2.7)
Liver	3.8	108	390	1	3.2	7.5(± 1.0)	2.4(± 0.5)	3.1(± 1.1)	6.5(± 1.4)
				2	3.8	2.3(± 0.3)	2.6(± 0.5)	0.9(± 0.6)	12.8(± 2.7)
				3	3.8	2.6(± 0.3)	2.8(± 0.6)	0.9(± 0.7)	13.6(± 2.8)
Liver	3.8	158	505	1	3.1	3.6(± 0.5)	2.0(± 0.4)	1.8(± 0.6)	5.8(± 1.2)
				2	3.8	6.9(± 0.9)	1.8(± 0.4)	3.8(± 1.0)	11.0(± 2.3)
				3	3.4	2.3(± 0.3)	1.8(± 0.5)	1.2(± 0.5)	11.1(± 2.3)

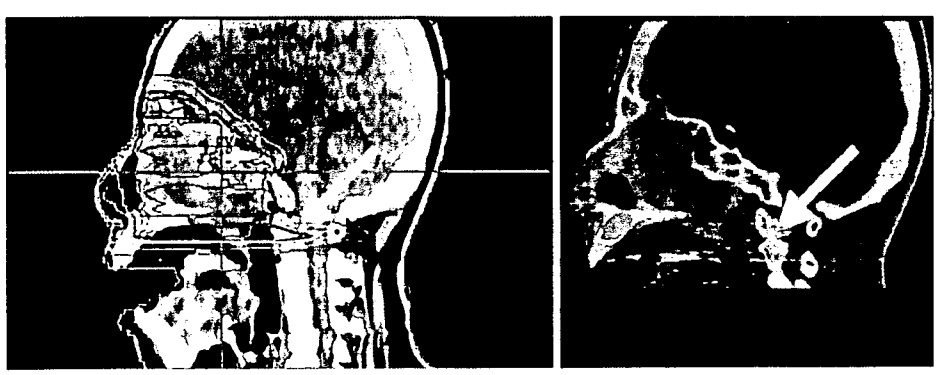

Fig. 8 Dose distribution and activity distribution on CT image after proton treatment of tumor in the head and neck. The *arrow* indicates the dose point of the spike shape

nuclear fragmentation reaction in a mono-energetic proton beam. Moreover, it was confirmed that the lateral activity distribution corresponds to the real beam size with an accuracy within 1 mm. In the therapeutic SOBP proton beam, the difference of the range between proton beam and the activity is larger than the case of a mono-energetic proton beam. Moreover, the therapeutic SOBP beam deteriorates the correspondence between the lateral dose and the activity distributions.

There is no simple relation between the stopping power of proton beam that determines the proton dose distribution and the cross section of the nuclear fragmentation reaction expressed as Eq. 1. Therefore, the activity distribution has no sharp peak like the Bragg peak in the proton dose distribution. For a proton therapy, it is very large impact to monitor the therapeutic proton dose distribution by use of the activity distribution in a patient. Therefore, it is necessary to innovatively research the physical reaction mechanism of the nuclear fragmentation reaction.

In the position of the proton-irradiated volume in the patient, the accuracy at the lateral dose and activity distributions will be about half cm, and the accuracy at the distal distributions cm order by the effects of the energy threshold for the nuclear fragmentation reaction and the SOBP width in the target organ without the respiratory motion (head and neck, etc). On the other hand, the accuracy at the lateral dose and activity distributions will be a few cm on the direction of the organ motion especially in the target organ with the respiratory motion (liver, etc) for the PET measurement without synchronization. In a proton treatment planning at our facility, planning target volume (PTV) has the margin of 3–10 mm in clinical target volume (CTV) by each treatment site. It will be visually confirmed whether gross tumor volume (GTV) is inside the proton-irradiated field.

4 Conclusion

In proton therapy, the proton-irradiated volume in the patient body was visually confirmed by measurement of the activity of the positron-emitting nuclei generated by the nuclear fragmentation reaction by use of the PET-CT apparatus. Moreover, verifications of the distribution and intensity of activity were performed for each body tissue composition. As yet, quantitative evaluations of the absolute activities remain.

To date, the acquisitions of PET and CT images were executed separately by use of each apparatus [7, 9]. There was a limit on the precision of image fusion. Therefore, determining whether the activity in the ribs or subcutaneous adipose tissue was high was previously very difficult after proton treatment of liver and lung cancers [7]. In this study, the confirmation of high activity in subcutaneous adipose tissue demonstrated the advantage of using PET-CT apparatus. The high activity in liver tumors, TACE may be used for dose-reference marker of the proton beam irradiation.

In the result, it was suggested that the events of the activity detected by use of the BOLPs provided enough data for reconstruction of the PET image. The clinical use of this information about the positron-emitting nuclei generated will be important for promoting proton treatment with higher accuracy in the future. For that reason, it will be necessary to much-improve the accuracy of the measured and calculated activity for the innovative proton therapy in which the irradiation position is especially controlled within a few mm in the treatment site with high accuracy of the patient positioning such as head and neck.

Acknowledgments We greatly thank the staff members of the Proton Radiotherapy Department of the National Cancer Center, Kashiwa, for their assistance, and the members of SHI Accelerator Service Ltd. and Accelerator Engineering Inc. for operation of the proton apparatus. We are grateful to the reviewers and editors of this Journal for their comments and advices, and thank the other office staffs for their supports.

References

1. Chu WT, Ludewigt BA, Renner TR. Instrumentation for treatment of cancer using proton and light-ion beams. Rev Sci Instrum. 1993;64(8):2055–122.
2. Bennett GW, Goldberg A, Levine G, Guthy J, Balsamo J. Beam localization via 15O activation in proton radiation therapy. Nucl Instr Meth. 1975;125:333–8.
3. Bennett GW, Archambeau JO, Archambeau BE, Meltzer JI, Wingate CL. Visualization and transport of positron emission from proton activation in vivo. Science. 1978;200:1151–3.
4. Oelfke U, Lam G, Atkins M. Proton dose monitering with PET: quantiative studies in Lucite. Phys Med Biol. 1996;41:177–96.
5. Litzenberg DW, Roberts DA, Lee MY, Pham K, Vander Molen AM, Ronningen R, et al. On-line monitoring of radiotherapy beams: experimental results with proton beams. Med Phys. 1999;26(6):992–1006.
6. Parodi K, Enghardt W. Potential application of PET in quality assuarnce of proton therapy. Phys Med Biol. 2000;45:N151–6.
7. Nishio T, Ogino T, Shimbo M, Katsuta S, Kawasaki S, Murakami T, et al. Distributions of β^+ decayed nucleus produced from the target fragment reaction in (CH_2) n and patient liver targets by using a proton beam for therapy. Abstracts of the XXXIV PTCOG MEETING in Boston; 2001. pp. 15–6.
8. Parodi K, Enghardt W, Haberer T. In-beam PET measurements of β^+ radioactivity induced by proton beams. Phys Med Biol. 2002;47:21–36.
9. Hishikawa Y, Kagawa K, Murakami M, Sasaki H, Akagi T, Abe M. Usefulness of positron-emission tomographic images after proton therapy. Int J Rad Oncol Biol Phys. 2002;53:1388–91.
10. Enghardt W, Crespo P, Fiedler F, Hinz R, Parodi K, Pawelke J, et al. Dose quantification from in-beam positron emission tomography. Radiother Oncol. 2004;73(Suppl. 2):S96–8.
11. Nishio T, Sato T, Kitamura H, Murakami K, Ogino T. Distributions of β^+ decayed nuclei generated in the CH_2 and H_2O

targets by the target nuclear fragment reaction using therapeutic MONO and SOBP proton beam. Med Phys. 2005;32(4):1070–82.
12. Parodi K, Ponisch F, Enghardt W. Experimental study on the feasibility of in-beam PET for accurate monitoring of proton therapy. IEEE Trans Nucl Sci. 2005;52:778–86.
13. Nishio T, Ogino T, Nomura K, Uchida H. Dose-volume delivery guided proton therapy using beam ON-LINE PET system. Med Phys. 2006;33(11):4190–7.
14. Photon, Electron, Proton and Neutron Interaction Data for Body Tissues (ICRU Report 46). pp. 11–3.
15. Iljinov AS, Semenov VG, Semenova MP, Schopper H. Interactions of protons with nuclei (supplement to I/13a, b, c), (Landolt-Bornstein New Series. 1994).
16. Goldharber AS. Statistical models of fragmentation processes. Phys Lett. 1974;53B:306–8.
17. Winger A, Sherrill BM. Morrissey. INTENSITY: acomputer program for the estimation of secondary beam intensities from a projectile fragment separator. Nucl Instrum Methods. 1992;B70:380–92.
18. Nishio T. Proton therapy facility at National Cancer Center, Kashiwa, Japan. J At Energy Soc. 1999;41(11):1134–8.
19. Tachikawa T, Sato T, Ogino T, Nishio T. Proton treatment devices at National Cancer Center (Kashiwa). Radiat Indust. 1999;84:48–53.
20. Nishio T, Kataoka S, Tachibana M, Matsumura K, Uzawa N, Saito H, et al. Development of a simple control system for uniform proton dose distribution in a dual-ring double scattering system. Phys Med Biol. 2006;51:1249–60.
21. Nishio T, Ogino T, Sakudo M, Tanizaki N, Yamada M, Nishida G, et al. Present proton treatment planning system at National Cancer Center Hospital East. Jpn J Med Phys Proc. 2000;20(Suppl. 4):174–7.
22. Boellaard R, Lingen AV, Lammertsma AA. Experimental and clinical evaluation of iterative reconstruction (OSEM) in dynamic PET: quantitative characteristics and effects on kinetic modeling. J Nucl Med. 2001;42:808–17.
23. Tomitani T, Pawelke J, Kanazawa M, Yoshikawa K, Yoshida K, Sato M, et al. Washout studies of ^{11}C in rabbit thigh muscle implanted by secondary beams of HIMAC. Phys Med Biol. 2003;48:875–89.
24. Mizuno H, Tomitani T, Kanazawa M, Kitagawa A, Pawelke J, Iseki Y, et al. Washout measurement of radioisotope implanted by radioactive beams in the rabbit. Phys Med Biol. 2003;48:2269–81.

Lung Cancer (2007) 56, 357–362

available at www.sciencedirect.com

ScienceDirect

journal homepage: www.elsevier.com/locate/lungcan

LUNG CANCER

Postoperative radiotherapy for non-small-cell lung cancer: Results of the 1999–2001 patterns of care study nationwide process survey in Japan

Takashi Uno[a,*], Minako Sumi[b], Ayaka Kihara[c], Hodaka Numasaki[c], Hiroyuki Kawakami[a], Hiroshi Ikeda[b], Michihide Mitsumori[d], Teruki Teshima[c],

Japanese PCS Working Subgroup of Lung Cancer

[a] *Department of Radiology, Graduate School of Medicine, Chiba University, Inohana 1-8-1, Chuou-ku, Chiba City, Chiba 260-8670, Japan*
[b] *Division of Radiation Oncology, National Cancer Center, Tokyo, Japan*
[c] *Department of Medical Physics and Engineering, Osaka University Graduate School of Medicine, Suita, Osaka, Japan*
[d] *Department of Therapeutic Radiology and Oncology, Graduate School of Medicine, Kyoto University, Kyoto, Japan*

Received 29 November 2006; received in revised form 4 January 2007; accepted 17 January 2007

KEYWORDS
Non-small-cell lung cancer;
Postoperative radiation therapy;
Patterns of care study;
Practice;
Survey;
PORT meta-analysis

Summary To investigate the practice process of postoperative radiation therapy for non-small-cell lung cancer (NSCLC) in Japan. Between April 2002 and March 2004, the Patterns of Care Study conducted an extramural audit survey for 76 of 556 institutions using a stratified two-stage cluster sampling. Data on treatment process of 627 patients with NSCLC who received radiation therapy were collected. Ninety-nine (16%) patients received postoperative radiation therapy between 1999 and 2001 (median age, 65 years). Pathological stage was stage I in 8%, II in 17%, IIIA in 44%, and IIIB in 20%. The median field size was 9 cm × 11 cm, and median total dose was 50 Gy. Photon energies of 6 MV or higher were used for 64 patients, whereas a cobalt-60 unit was used for five patients. Three-dimensional conformal treatment was used infrequently. Institutional stratification influenced several radiotherapy parameters such as photon energy and planning target volume. Smaller non-academic institutions provided worse quality of care. The study confirmed continuing variation in the practice of radiotherapy according to stratified institutions. Outdated equipment such as Cobalt-60 units was used, especially in non-academic institutions treating only a small number of patients per year.

* Corresponding author. Tel.: +81 43 226 2100; fax: +81 43 226 2101.
E-mail address: unotakas@faculty.chiba-u.jp (T. Uno).

0169-5002/$ – see front matter © 2007 Elsevier Ireland Ltd. All rights reserved.
doi:10.1016/j.lungcan.2007.01.017

1. Introduction

Postoperative radiation therapy (PORT) decreases the risk of local–regional recurrence in patients with resected non-small-cell lung cancer (NSCLC) [1–3]. However, reduction in the frequency of local recurrence has not translated into a survival benefit in most studies. In 1998, the impact of PORT for NSCLC was analyzed in a meta-analysis of phase III trials [4]. After publication of the PORT meta-analysis, which emphasized deleterious effects in patients receiving PORT for completely resected N0-1 cases, much of the clinical focus on adjuvant therapy shifted to chemotherapy [5,6]. Thus, the role of PORT for patients at high risk for locoregional failure such as those with N2 disease remains unclear. Adjuvant chemotherapy trials have often permitted use of PORT as an option for patients with N2 disease [5,7]. One clinical study reported promising results for combined PORT and chemotherapy for patients with pathologic stage II or IIIA disease [8]. The results of these trials imply that PORT delivered using modern radiotherapy techniques may potentially provide a survival advantage for selected high-risk patients.

The Patterns of Care Study (PCS) is a retrospective study designed to investigate the national practice for cancer patients during a specific period [9,10]. In April 2002, the PCS started a nationwide survey for patients with NSCLC treated with radiation therapy in Japan. In the present report, we provide results of analyses focused on patients who received PORT for NSCLC during the study period. The objectives of this study were to reveal clinical practice patterns regarding PORT after publication of the PORT meta-analysis and to assess variation in clinical practice according to stratified institutions.

2. Materials and methods

Between April 2002 and March 2004, the PCS conducted a national survey of radiation therapy for patients with lung cancer in Japan. The Japanese PCS developed an original data format and performed an extramural audit survey for 76 of 556 institutions using a stratified two-stage cluster sampling. Data collection consisted of two steps of random sampling. Prior to random sampling, all institutions were classified into one of four groups. Criteria for stratification have been described elsewhere [10]. Briefly, the PCS stratified Japanese institutions as follows: A1, academic institutions such as university hospitals or national/regional cancer center hospitals treating $\geqq 430$ patients per year; A2, academic institutions treating <430 patients; B1, non-academic institutions treating $\geqq 130$ patients per year; and B2, <130 patients. The cut-off values in number of patients treated per year between A1 and A2 institutions and B1 and B2 institutions, respectively, were increased from those used in the previous PCS study because of the increase in the number of patients treated by radiation therapy in Japan [10]. Eligible patients had 1997 International Union Against Cancer (UICC) stage I–III NSCLC that was treated with PORT between 1999 and 2001, a Karnofsky Performance Status (KPS) >50 prior to start of treatment, and no evidence of other malignancies within 5 years. The current PCS collected specific information on 627 patients (A1:157, A2:117, B1:214, B2:139) who were treated with radiation therapy between 1999 and 2001. Of those, 99 (16%) patients (A1:15, A2:17, B1:45, B2:22) who received PORT constitute the subjects of the present analysis. The practice of PORT was investigated by reviewing items in each medical chart such as demographics, symptoms, history, work-up examinations, pathology, clinical stage, treatment course including radiation therapy, surgery and chemotherapy, and radiotherapy parameters. In addition, simulation films and linacgraphy of each patient were also reviewed by surveyors.

The PCS surveyors consisted of 20 board-certified radiation oncologists. For each institution, one radiation oncologist visited and surveyed data by reviewing patient charts. In order to validate the quality of collected data, the PCS utilized an internet mailing-list among all surveyors. In situ real-time check and adjustment of data input were available between each surveyor and the PCS committee. In tables, "missing" indicates that the item in the data format was left empty, whereas "unknown" means that the item in the format was completed with data "unknown". We combined "missing" and "unknown" in tables because their meanings were the same in most cases; no valid data were obtained in the given resources. Cases with missing or unknown values were included when both the percentage and significance value were calculated. Statistical significance was tested by the χ^2 test. A p-value less than 0.05 was considered statistically significant. Overall survival was assessed from the day of surgery and was estimated by the Kaplan–Meier product limit method using the Statistical Analysis System, Version 6.12.

3. Results

3.1. Patient and tumor characteristics

Patient and clinical tumor characteristics are shown in Table 1. Of the 99 patients who received PORT, 32 were treated at academic institutions and 67 at non-academic institutions. The proportion of patients with NSCLC who received PORT was significantly higher in non-academic institutions than in academic institutions (19% versus 12%, $p = 0.013$). Overall, median age was 65 years (range, 39–82), and the male to female ratio was 4:1. Ninety-three percent of patients had a KPS greater than or equal to 80%. Preoperative examinations included chest computed tomography (CT) in 97% of patients, bronchoscopy in 87%, brain CT or magnetic resonance imaging (MRI) in 75%, abdominal CT in 75%, bone scintigraphy in 83%, and mediastinoscopy in 4%. The primary tumor site was the upper lobe in 62 patients, middle lobe in 7, and lower lobe in 27. The remaining 2 patients had a primary tumor near the border of the upper and middle lobes that involved both lobes, and they were allocated to "others". Peripheral tumors were twice as common as central tumors. When tumors were analyzed by laterality, the ratio of right to left side primary site was 1.5. Clinical T- and N-classifications were T1 in 28 patients, T2 in 35, T3 in 24, T4 in 11, and N0 in 33, N1 in 19, N2 in 40, and N3 in 6, resulting in clinical stage I in 27 patients, II in 14, IIIA in 41, and IIIB in 16. The numbers less than 99 are due to missing or unknown data.

Table 1 Patient and tumor characteristics

No. of patients	99
Men	79
Women	20
Age (years)	
Median	65
Range	32–89
% KPS ≥ 80	93
Preoperative work-up (%)	
Chest CT	97
Bronchoscopy	87
Brain CT or MRI	75
Abdominal CT	75
Bone scan	83
Mediastinoscopy	4
Primary tumor site	
Upper lobe	62
Middle lobe	7
Lower lobe	27
Other	2
Missing	1
Tumor location	
Central	30
Peripheral	60
Missing	9
Laterality	
Left lung	38
Right lung	59
Missing	2
Clinical T factor	
TX	1
T1	28
T2	35
T3	24
T4	11
Clinical N factor	
NX	1
N0	33
N1	19
N2	40
N3	6
Clinical stage	
IA	14
IB	13
IIA	7
IIB	7
IIIA	41
IIIB	16
Missing	1

KPS, Karnofsky performance status score.

3.2. Surgery and tumor pathology characteristics (Table 2)

The primary surgical procedure was a lobectomy in 78 patients, pneumonectomy in 12, and segmentectomy in 9.

Table 2 Surgical procedure and tumor pathology characteristics

Type of surgery	
Lobectomy	78
Pneumonectomy	12
Segmentectomy	9
Histopathology	
Squamous cell carcinoma	47
Adenocarcinoma	43
Large cell carcinoma	7
Adenosquamous carcinoma	2
Surgical margin status	
Negative	55
Positive	31
Missing	13
Pathological T factor	
T1	22
T2	35
T3	23
T4	18
Missing	1
Pathological N factor	
N0	15
N1	19
N2	56
N3	4
Missing	5
Pathologically involved mediastinal nodes (%)[a]	
No. 1	16
No. 2	23
No. 3	26
No. 4	34
No. 5	28
No. 6	5
No. 7	34
No. 8	12
Pathological stage	
IA	4
IB	5
IIA	9
IIB	8
IIIA	45
IIIB	20
Missing/unknown	8

[a] Nearly half of the data for this item were "missing/unknown".

Among all 99 patients, complete resection was accomplished for 55 patients. Surgical margin status was positive in 31 patients. Histopathology was squamous cell carcinoma in 47 patients, adenocarcinoma in 43, large cell carcinoma in 7, and adenosquamous carcinoma in 2. Predominantly involved mediastinal nodes confirmed pathologically to contain tumor were No. 7 (34%), No. 4 (34%), No. 5 (28%), and No. 3 (26%) according to the lymph node mapping system of the Japan Lung Cancer Society [11], although nearly half of the data for this item were "missing/unknown." The pathological T-

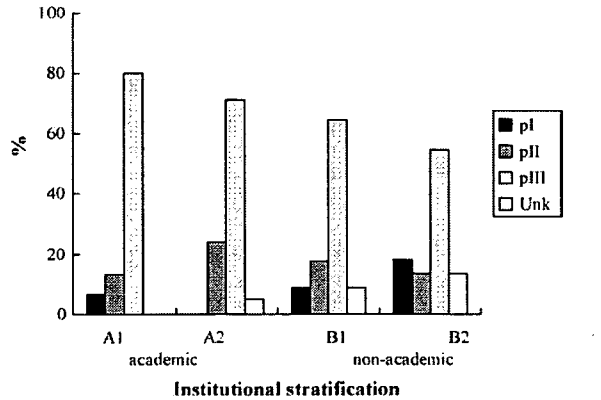

Fig. 1 Proportion of patients with pathologic stage III disease tended to be higher in large academic institutions ($p = 0.13$).

Table 3 Pathological stage in patients with complete surgery according to the stratified institution

Pathological stage	Institutional stratification				Total
	A1	A2	B1	B2	
I–II	2	4	8	4	18
III	5	6	18	8	37
Total	7	10	26	12	55

and N-classifications were pT1 in 22 patients, pT2 in 35, pT3 in 23, and pT4 in 18, and pN0 in 15 patients, pN1 in 19, pN2 in 56, and pN3 in 4. Pathological stage was stage I in 9 patients, II in 17, IIIA in 45, and IIIB in 20, respectively. The proportion of pathological stage III patients tended to be higher in large academic institutions (Fig. 1, $p = 0.13$). Breakdown of pathological stage in 55 patients who underwent complete surgery according to the stratified institution group was shown in Table 3. As for the proportion of pathological stage III patients, no significant difference was observed between institutions.

3.3. Radiotherapy parameters (Table 4)

A CT-simulator was used for planning for 26 patients. Ninety-one patients were treated with opposed AP-PA fields, and field reduction during the course of radiotherapy was done for 48%. Three-dimensional treatment was used in only 2 patients. Photon energies of less than 6 MV were used for 34 patients (34%). Dose prescription by isodose line technique was performed for only 8 patients (8%). The median field size was 9 cm × 11 cm, and the median total dose was 50 Gy. The planning target volume included the ipsilateral hilus in 80%, ipsilateral mediastinum in 86%, contralateral mediastinum in 68%, contralateral hilus in 9%, ipsilateral supraclavicular region in 30%, and contralateral supraclavicular region in 22%. Institutional stratification was found to influence several radiotherapy parameters. A photon energy of 6 MV or higher was used for 73% of patients in A1, 77% in A2, and 80% in B1 institutions, whereas it was used for only 23% of patients in B2 institutions (Fig. 2, $p < 0.0001$). A Cobalt-60 unit was used only in 5 B2 institutions. The planning target volume included the contralateral mediastinum for more than 70% of patients in A1 to B1 institutions, whereas it was included in only 46% of patients treated in B2 institutions ($p = 0.011$).

Table 4 Radiotherapy parameters

Simulation method	
CT-simulator	26
X-ray simulator	38
X-ray simulator + CT	26
Missing	7
Treatment technique	
AP-PA	91
Oblique	2
Three-field	1
Three-dimensional conformal	2
Other	2
Missing	1
Photon energy	
60 Co	5
<6 MV	29
≥6 MV	64
Missing	1
Dose prescription	
Isodose line	8
Point	91
Total dose	
≤3000 cGy	1
3001–4000 cGy	6
4001–5000 cGy	49
5001–6000 cGy	37
6001–7000 cGy	6
Missing	1
Median total dose (cGy)	5000
All fields treated each day (%)	83
Median field size (cm)	
Left-right	9 (range, 5–23)
Cranio-caudal	11 (range, 5–20)
Field reduction during radiotherapy (%)	48
Field included (%)	
Ipsilateral hilus	80
Ipsilateral mediastinum	86
Contralateral mediastinum	68
Contralateral hilus	9
Ipsilateral supraclavicula	30
Contralateral supraclavicula	22

3.4. Use of chemotherapy

Thirty patients (31%) received systemic chemotherapy. For 21 patients, chemotherapy and PORT were administered concurrently, mainly using a platinum-based, two-drug combination. For 9 of the 30 patients, platinum-based chemotherapy was used as induction therapy. Oral fluorouracil was used for 9 patients.

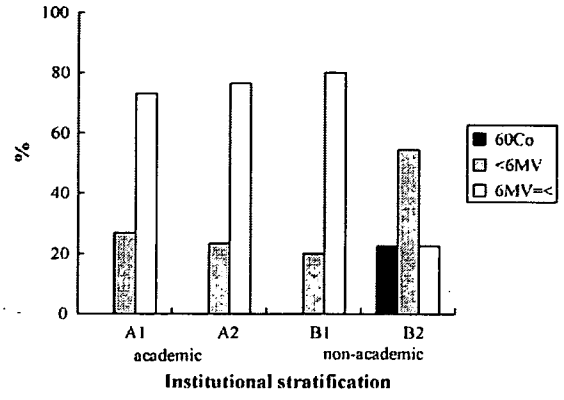

Fig. 2 A photon energy of 6 MV or higher was used for 73% of patients in A1 institutions, 77% in A2, and 80% in B1, whereas only 23% in B2 institutions ($p < 0.0001$). A Cobalt-60 unit was used only in B2 institutions.

3.5. Failure pattern and preliminary clinical outcome

The site of first failure was local in 6, regional in 5, and distant in 31. Of the patients who developed failure, the median time to first failure was 7 months. Although the current PCS has limitations in terms of outcome analysis due to a short follow-up period and significant variations in follow-up information according to institutional stratification [10,12], overall survival for the entire group was 88% at 1 year and 63% at 3 years, with a median follow-up period after PORT of 1.7 years.

4. Discussion

The results of the present PCS reflect national practices for PORT for NSCLC in Japan. However, when interpreting our data, it is important to note that they were limited to patients who received radiation therapy. We have no information about patients who did not receive radiation therapy after surgery. Thus, we have no data concerning the percentage of patients who underwent radiation therapy after surgery. Analysis of the national practice process for all patients with NSCLC in the adjuvant setting is beyond the scope of this study.

All eligible patients in this study received radiation therapy after publication of the PORT meta-analysis that emphasized deleterious effects in patients receiving PORT, especially for patients with completely resected N0-1 disease [4]. Since then, the clinical focus on adjuvant treatment has largely shifted to chemotherapy, which has become part of the postoperative standard of care for patients with NSCLC [5,6,8]. In the United States, use of PORT has substantially declined due to the lack of proven survival benefit [13]. However, PORT was still incorporated as an option in recent clinical trials that recruited patients with pathological N2 disease [5,7]. The recent analysis of Surveillance, Epidemiology, and End Results (SEER) data in the United States demonstrated that PORT was associated with improved survival for patients with N2 disease [14,15]. In addition, a recent clinical study has reported promising results for combined PORT and chemotherapy using modern radiotherapy techniques [7,8]. Thus, the current clinical question is whether adjuvant chemotherapy combined with PORT improves survival for patients at high risk for locoregional failure compared with adjuvant chemotherapy alone. Taking all of the evidence together, we conclude that PORT still plays an important role in the adjuvant setting. We believe that this PCS study provides basic data of current practice regarding PORT in Japan.

Results of the present study demonstrated that patients who received PORT accounted for 16% of all patients with NSCLC who received radiation therapy in Japan between 1999 and 2001. Of all 99 patients, 65 had pathological stage III disease (45, stage IIIA; 20, stage IIIB). Using a median field size of 9 cm × 11 cm, a median total dose of 50 Gy was delivered mainly through opposed AP-PA fields. Three-dimensional conformal treatment was infrequently used. Field size reduction during the course of radiotherapy was done for almost half of the patients. A dedicated CT-simulator was used for 26 patients. The PORT meta-analysis was criticized because the authors included several old studies in which a cobalt machine was used for radiotherapy. It was pointed out that suboptimal administration of PORT using outdated techniques counterbalanced the beneficial locoregional effects of PORT treatment in the meta-analysis [16]. Because of potential pulmonary/cardiac toxic effects of mediastinal radiotherapy, PORT should be delivered with modern radiotherapy techniques using CT-based three-dimensional conformal treatment planning, a technique with which target volumes and normal tissue constraints are precisely defined. Although the patients included in this PCS survey were treated between 1999 and 2001, the modern radiotherapy era, 34% of all patients were treated using photon energies <6 MV, including five patients who were treated using a cobalt machine. Institutional stratification influenced several radiotherapy parameters in PORT for NSCLC. As shown in the previous report for small-cell lung cancer in Japan [17], smaller non-academic institutions (B2) provided a lower quality of care for their patients. Planning target volume typically included the ipsilateral hilus, ipsilateral mediastinum, and contralateral mediastinum in A1 to B1 institutions, whereas the contralateral mediastinum was included for only 46% of patients treated in B2 institutions. Although there is controversy concerning prophylactic nodal irradiation in the setting of definitive radiation therapy, PORT for patients with pN2 NSCLC should include the contralateral mediastinum. Proportion of patients with pathological stage I–II who underwent complete surgery did not differ between stratified institution groups. Thus, it was considered that omission of treating the contralateral mediastinum in B2 institutions was not caused by unbalance in stage distribution. We speculate that this discrepancy in care was due mainly to the extremely small number of radiation oncologists in B2 institutions. We also found that obsolete equipment such as Cobalt-60 units were still used, especially in non-academic institutions treating only a small number of patients per year. The proportion of patients treated with 6 MV or higher photon energies was significantly higher in A1 to B1 institutions than in B2 institutions. A Cobalt-60 unit was used only in B2 institutions. The present study again confirms differences in the practice of radiotherapy according to institutional stratification status.

We consider that the structure of radiation oncology is a domestic problem specific to each country. The results represent intrinsic problems with the structure of radiation therapy in Japan. Considering the current immaturity of the Japanese structure of radiation oncology, PCS still perform an important role in monitoring structure and process, as well as providing essential information not only to medical staff and their patients but also to administrative policy makers.

5. Conclusions

Through the audit survey and subsequent data analyses, the PCS established nationwide basic information on the practice of PORT for NSCLC in Japan. Even after the publication of the PORT meta-analysis, PORT was used for a considerable proportion of patients receiving radiotherapy. However, this PCS documented that outdated modalities such as cobalt-60 units were still used in small non-academic institutions during the study time frame. Thus, the current PCS confirmed the continuing existence of variation in the practice of radiotherapy according to institution stratification.

Conflict of interest

We have no conflict of interest in connection with this paper.

Acknowledgments

This study was presented in part at the Second USA/Japan PCS Workshop, in Tokyo, Japan, on February 17–19, 2003 and in part at the 13th European Cancer Conference, in Paris, France, on October 30–November 3. The authors thank all radiation oncologists and staff who participated in this study for their support and cooperation. This study was supported by the following grants: Ministry of Health, Labor and Welfare (Grants-in-Aid for Cancer Research nos. 10-17 and 14-6); Japan Society for Promotion of Sciences; and the Research Fund in 1999 and 2000 from the Japan Society of Therapeutic Radiology and Oncology.

References

[1] The Lung Cancer Study Group. Effects of postoperative mediastinal radiation on completely resected stage II and stage III epidermoid cancer of the lung. N Engl J Med 1986;315:1377–81.

[2] Mayers R, Smolle-Juettner FM, Szolar D, Stuecklschweiger GF, Quehenberger F, Friehs G, et al. Postoperative radiotherapy in radically resected non-small-cell lung cancer. Chest 1997;112:954–9.

[3] Feng QF, Wang M, Wang LJ, Yang ZY, Zhang YG, Zhang DW, et al. A study of postoperative radiotherapy in patients with non-small cell lung cancer: a randomized trial. Int J Radiat Oncol Biol Phys 2000;47:925–9.

[4] PORT Meta-analysis Trialists Group. Postoperative radiotherapy in non-small-cell lung cancer: systemic review and meta-analysis of individual patient data from nine randomized controlled trials. Lancet 1998;352:257–63.

[5] The International Adjuvant Lung Cancer Trial Collaborative Group. Cisplatin-based adjuvant chemotherapy in patients with completely resected non-small cell lung cancer. N Engl J Med 2004;350:351–60.

[6] Winton T, Livingston R, Johnson D, Rigas J, Johnston M, Butts C, et al. Vinorelbine plus cisplatin vs. observation in resected non-small-cell lung cancer. N Engl J Med 2005;352:2589–97.

[7] Douillard J-Y, Rosell R, De Lena M, Carpagnano F, Ramlau R, Gonzales-Larriba JL, et al. Adjuvant vinorelbine plus cisplatin versus observation in patients with completely resected stage IB-IIIA non-small-cell lung cancer (Adjuvant Navelbine International Trialist Association [ANITA]): a randomized controlled trial. Lancet Oncol 2006;7:719–27.

[8] Bradley JD, Paulus R, Graham MV, Ettinger DS, Johnstone DW, Pilepich MV, et al. Phase II trial of postoperative adjuvant paclitaxel/carboplatin and thoracic radiotherapy in resected stage II and IIIA non-small-cell lung cancer: promising long-term results of the Radiation Therapy Oncology Group—RTOG 9705. J Clin Oncol 2005;23:3480–7.

[9] Hanks GE, Coia LR, Curry J. Patterns of care studies. Past, present and future. Semin Radiat Oncol 1997;7:97–100.

[10] Teshima T. Japanese PCS Working Group. Patterns of Care Study in Japan. Jpn J Clin Oncol 2005;35:497–506.

[11] Naruke T, Suemasu K, Ishikawa S. Lymph node mapping and curability at various levels of metastasis in resected lung cancer. J Thorac Cardiovasc Surg 1978;76:832–9.

[12] Sugiyama H, Teshima T, Ohno Y, Inoue T, Takahashi Y, Oshima A, et al. The patterns of care study and regional cancer registry for non-small-cell lung cancer in Japan. Int J Radiat Oncol Biol Phys 2003;56:1005–12.

[13] Bekelman J, Rosenzweig KE, Bach PB, Schrag D. Trends in the use of postoperative radiotherapy for resected non-small-cell lung cancer. Int J Radiat Oncol Biol Phys 2006;66:492–9.

[14] Rescigno J. Use of postoperative radiotherapy for node-positive non-small-cell lung cancer. Clin Lung Cancer 2002;4:35–44.

[15] Lally BE, Zelterman D, Colasanto JM, Haffty BG, Detterbeck FC, Wilson LD. Postoperative radiotherapy for stage II or III non-small-cell lung cancer using the Surveillance, Epidemiology, and End Results database. J Clin Oncol 2006;24:2998–3006.

[16] Bogart JA, Aronowitz JN. Localized non-small cell lung cancer: adjuvant radiotherapy in the era of effective systemic therapy. Clin Cancer Res 2005;11(Suppl. 13):5004s–10s.

[17] Uno T, Sumi M, Ikeda H, Teshima T, Yamashita M, Inoue T, et al. Radiation therapy for small-cell lung cancer: results of the 1995–1997 patterns of care process survey in Japan. Lung Cancer 2002;35:279–85.

Jpn J Clin Oncol 2007;37(3)175–180
doi:10.1093/jjco/hym008

Phase I Study of Cisplatin Analogue Nedaplatin, Paclitaxel, and Thoracic Radiotherapy for Unresectable Stage III Non-Small Cell Lung Cancer

Ikuo Sekine[1], Minako Sumi[2], Yoshinori Ito[2], Terufumi Kato[1], Yasuhito Fujisaka[1], Hiroshi Nokihara[1], Noboru Yamamoto[1], Hideo Kunitoh[1], Yuichiro Ohe[1] and Tomohide Tamura[1]

[1]Divisions of Internal Medicine and Thoracic Oncology and [2]Radiation Oncology, National Cancer Center Hospital, Tokyo, Japan

Received September 6, 2006; accepted November 1, 2006; published online April 23, 2007

Background: The standard treatment of unresectable stage III non-small cell lung cancer is concurrent chemoradiotherapy in patients in good general condition, but where the optimal chemotherapeutic regimen has not been determined.
Methods: Patients with unresectable stage III non-small cell lung cancer received nedaplatin (80 mg/m^2) and paclitaxel on day 1 every 4 weeks for 3–4 cycles and concurrent thoracic radiotherapy (60 Gy/30 fractions for 6 weeks) starting on day 1. The dose of paclitaxel was escalated from 120 mg/m^2 in level 1, 135 mg/m^2 in level 2 to 150 mg/m^2 in level 3.
Results: A total of 18 patients (14 males and 4 females, with a median age of 62.5 years) were evaluated in this study. Full cycles of chemotherapy were administered in 83% of patients in level 1, and in 50% of patients in levels 2 and 3. No more than 50% of patients developed grade 4 neutropenia. Transient grade 3 esophagitis and infection were noted in one patient, and unacceptable pneumonitis was noted in three (17%) patients, two of whom died of the toxicity. Dose-limiting toxicity (DLT), evaluated in 15 patients, noted in one of the six patients in level 1, three of the six patients in level 2 and one of the three patients in level 3. One DLT at level 2 developed later as radiation pneumonitis. Thus, the maximum tolerated dose was determined to be level 1. The overall response rate (95% confidence interval) was 67% (41–87%) with 12 partial responses.
Conclusion: The doses of paclitaxel and nedaplatin could not be escalated as a result of severe pulmonary toxicity.

Key words: non-small cell lung cancer – chemoradiotherapy – paclitaxel – nedaplatin – pneumonitis

INTRODUCTION

Locally advanced unresectable non-small cell lung cancer (NSCLC), stage IIIA disease with bulky N2 and stage IIIB disease without pleural effusion, is characterized by large primary lesions, and/or involvement of the mediastinal or supraclavicular lymph nodes, and occult systemic micrometastases (1). Concurrent chemoradiotherapy, recently shown to be superior to the sequential approach in phase III trials, is the standard medical care for this disease (2–4). Chemotherapy regimens used concurrently with thoracic radiotherapy in these randomized trials were second-generation platinum-based chemotherapy, such as combinations of cisplatin, vindesine and mitomycin, cisplatin and vinblastine, and cisplatin and etoposide. The third-generation cytotoxic agents including vinorelbine and paclitaxel, which provided a better survival rate in patients with disseminated disease than second-generation agents, must be reduced when administered concurrently with thoracic radiotherapy (5–7). Thus, the optimal chemotherapy for concurrent chemoradiotherapy has not been established.

Nedaplatin (*cis*-diammine-glycolate-O,O′-platinum II, 254-S) is a second-generation platinum derivative that has an

For reprints and all correspondence: Ikuo Sekine, Division of Internal Medicine and Thoracic Oncology, National Cancer Center Hospital, Tsukiji 5-1-1, Chuo-ku, Tokyo 104-0045, Japan. E-mail: isekine@ncc.go.jp